Lawrence Berkeley National Laboratory
LBL Publications

Title
ELECTRICAL AND THERMAL PORPERTIES OF NEUTRON TRANSMUTION DOPED GE AND SO MK

Permalink
https://escholarship.org/uc/item/8jh8z3gq

Authors
Wang, N.
Wellstood, F.C.
Sadoulet, B.

Publication Date
1989-03-01

eScholarship.org Powered by the California Digital Library
University of California

UC-413
LBL-26884
Preprint

Lawrence Berkeley Laboratory
UNIVERSITY OF CALIFORNIA

Physics Division

RECEIVED
LAWRENCE
BERKELEY LABORATORY
JUL 3 1989
LIBRARY AND
DOCUMENTS SECTION

Submitted to Physical Review B

Electrical and Thermal Properties of Neutron Transmution Doped Ge at 20 mK

N. Wang, F.C. Wellstood, B. Sadoulet,
E.E. Haller, and J. Beeman

March 1989

For Reference

Not to be taken from this room

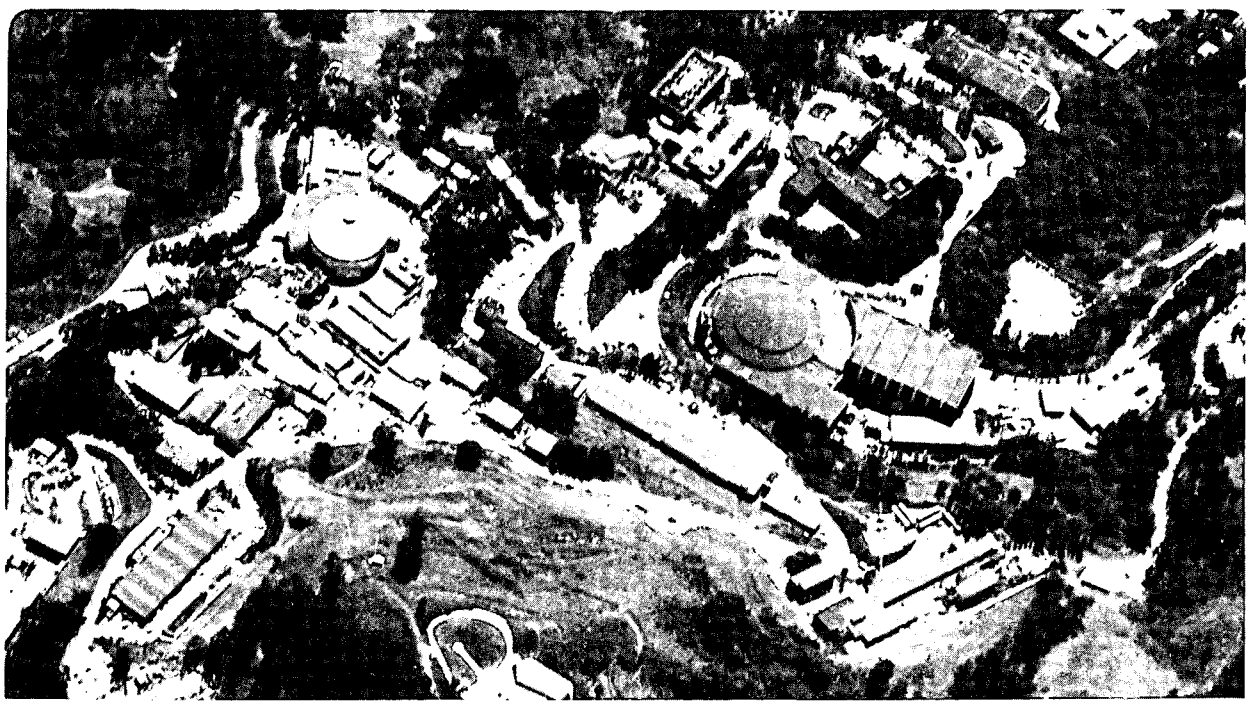

Prepared for the U.S. Department of Energy under Contract Number DE-AC03-76SF00098.

LBL-26884

DISCLAIMER

This document was prepared as an account of work sponsored by the United States Government. While this document is believed to contain correct information, neither the United States Government nor any agency thereof, nor the Regents of the University of California, nor any of their employees, makes any warranty, express or implied, or assumes any legal responsibility for the accuracy, completeness, or usefulness of any information, apparatus, product, or process disclosed, or represents that its use would not infringe privately owned rights. Reference herein to any specific commercial product, process, or service by its trade name, trademark, manufacturer, or otherwise, does not necessarily constitute or imply its endorsement, recommendation, or favoring by the United States Government or any agency thereof, or the Regents of the University of California. The views and opinions of authors expressed herein do not necessarily state or reflect those of the United States Government or any agency thereof or the Regents of the University of California.

LBL-26884

Electrical and Thermal Properties of Neutron Transmutation Doped Ge at 20 mK[1]

N. Wang, F.C. Wellstood, B. Sadoulet
Department of Physics, University of California, Berkeley and
Physics Division, Lawrence Berkeley Laboratory,
1 Cyclotron Rd, Berkeley, CA 94720

E.E. Haller
Department of Material Science and Mineral Engineering
University of California, Berkeley and
Engineering Division and Materials & Chemical Sciences Division
Lawrence Berkeley Laboratory
1 Cyclotron Rd, Berkeley, CA 94720

J. Beeman
Materials and Chemical Sciences Division
Lawrence Berkeley Laboratory
1 Cyclotron Rd, Berkeley, CA 94720

March 1989

[1]This work is supported in part by the Director, Office of Energy Research, Office of High Energy and Nuclear Physics, Division of High Energy Physics of the U.S. Department of Energy under Contract DE-AC03-76SF00098

Electrical and Thermal Properties of Neutron Transmutation Doped Ge at 20 mK

Ning Wang, F.C.Wellstood, B.Sadoulet

Department of Physics and Lawrence Berkeley Laboratory

E.E.Haller

Department of Material Science and Mineral Engineering and

Lawrence Berkeley Laboratory

J.Beeman

Lawrence Berkeley Laboratory

University of California, Berkeley, CA 94720

Abstract

We have measured the thermal and electrical properties of thermistors made of neutron transmutation doped Ge near 20 mK. The observed nonlinear I-V curves of these thermistors and their dynamic behavior are well explained by a thermal model, which is based on the decoupling of charge carriers and thermal phonons.

PACS numbers: 63.20.Kr, 66.70.+f, 72.10.Di, 72.20.Ht

1. Introduction

Neutron transmutation doped Ge (NTD Ge) has been successfully used by a variety of experimenters: infrared astronomers have used this material as a bolometer at 1K[1]; D. McCammon, *et al.*,[2] have developed a low threshold and high resolution (11eV FWHM) calorimeter using implanted silicon operating at 100 mK; and E. Fiorini and coworkers[3] have demonstrated a low threshold calorimeter using doped Ge as a temperature sensor at 30 mK.

The principle behind these calorimeters is that when a semiconducting material, such as Ge and Si, is doped with acceptor and/or donor atoms to a high enough concentration, the electrical conduction at low temperatures is dominated by variable range hopping. An exponential temperature dependence for the electrical resistivity is expected in this conduction regime.[4] This strong temperature dependence makes a doped semiconductor material very sensitive to temperature variations.

In order to detect dark matter particles in the laboratory, a calorimeter operating near 20 mK is required.[5] Even though NTD Ge has been successfully used down to about 300 mK, its properties at much lower temperatures are not experimentally established.

In this paper, we present results of measurements of the electrical and thermal properties of NTD Ge at dilution refrigerator temperatures (19 - 80 mK). We first describe the sample preparation. We then present the experimental setup and results of DC measurements, and propose a thermal model, which explains the observed nonlinear I-V curves. Following that we describe the experimental setup and the results of AC measurements, where we show the estimated temperature dependence of the heat capacities. We close with a brief discussion and conclusions.

2. Sample Preparation

Our NTD Ge is fabricated from ultrapure single-crystal Ge. Wafers 2-3 mm thick are cut from a 3-4 cm diameter single crystal and are exposed to a thermal neutron source. The technique of neutron transmutation doping[6] is based on the fact that Ge has isotopes that decay into dopant impurities after capture of thermal neutrons. This technique is expected to give a dopant concentration that is spatially more uniform than implantation or diffusion doping. The desired dopant concentration is achieved by controlling the neutron flux. Thermal annealing at 400^0 C for one hour is required to remove the radiation damage produced by fast neutrons. After neutron exposure and annealing, a strip about 300 μm

thick is cut from the wafer, and is B^+ implanted ($3x10^{14}$ cm^{-2}) to a depth of about 200 nm from both sides. The implanted layers are doped to such a high concentration that the semiconductor becomes metallic. After B^+ implantation doping, a layer of Pd of approximately 20 nm thick is sputtered onto the strip and followed by a Au layer of 400 nm. The strip is annealed again at 250^0 C for one hour to activate the implant. The function of the Pd is to form a strongly adhering layer between the Ge and the Au.

The sample arrangement is shown in Fig. 1 . The thermistor material, which we refer to as NTD Ge #12,[6] has a net dopant concentration N_A-N_D= $6.64x10^{16}$ cm^{-3}, where N_A is the number of acceptors per unit volume and N_D is the number of donors per unit volume. The compensation ratio (acceptor concentration/donor concentration) is 0.32. The chip dimensions are 1mmx3mmx0.2mm, and there are two thermistors made on the same chip. One is thermally clamped by gluing directly to a thermal sink with silver epoxy. The resistance of the thermally clamped thermistor is denoted as R_a, and the other as R_b. Both thermistors have the same geometry, consisting of two $1mm^2$ Au patches on opposite sides of the chip. The thermistors are separated by 1mm on the chip.

This arrangement was chosen because a double-thermistor sample enables us to monitor the lattice temperature of the sample with one thermistor while the other thermistor is being heated. Moreover, the arrangement also allows us to determine the thermal conductance between the phonons in the sample and those in the sink.[7]

The thermal sink consists of a Cu-Kapton-Cu sandwich (the Kapton thickness is 200 μm and the Cu area is about $1cm^2$). This sandwich is soldered with a thin layer of In to a Cu sample holder, which in turn is screwed to the mixing chamber of a dilution refrigerator. In order to eliminate any extra heat flow to the sample, electrical connections are made with 17.5μm diameter Al wires which are bonded ultrasonically to the three Au patches that are not heat sunk. Aluminum is superconducting below 1K and is a poor heat

conductor. The thermal conductance of such a wire of 1 cm length at 20 mK is estimated to be about 2×10^{-12} W/K. A Cu wire 25 μm in diameter is soldered with Sn-Pb alloy to the heat sunk patch. The sample is enclosed in a Cu box which acts as an electromagnetic shield.

3. DC Measurements and Results

3.1 Experimental Setup and Method

The circuit used in the current-voltage (I-V) measurements is shown in Fig. 2. Because the thermistors are extremely sensitive to radio frequency (rf) radiation (10^{-14} W of power changes the I-V curve significantly), measurements have been performed on a dilution refrigerator located in a screen room (made of Cu mesh) with rf filters on all the leads to the sample . In order to reduce any additional external sources of noise, the amplifiers, which are also located inside the screen room, and the current source are powered by batteries.

An I-V curve is obtained by varying the bias voltage and recording the voltages across the bias resistor and the thermistor simultaneously on an X-Y plotter. In order to eliminate errors from thermoelectric voltages, we record an I-V curve for both polarities of the bias voltage, and we use the center of symmetry point as the origin of the I-V curve; all I-V curves are highly symmetric with respect to this point. To measure resistance as a function of temperature, I-V curves are recorded at various mixing chamber temperatures for both thermistors. The temperature of the mixing chamber was measured with a carbon resistor that has been calibrated with a ^{60}Co source and with a SQUID noise thermometer.

3.2 Zero Bias Resistance

I-V curves of thermistor a are shown in Fig. 3. Notice that the zero bias resistance changes rapidly with the mixing chamber temperature as expected. However, the curves

are very nonlinear. At 19 mK a nonlinearity is observable at a current of 20 pA, when the power dissipated in the thermistor from the bias current is only 10^{-14} W.

The zero bias resistance, R(T), is measured as the slope of an I-V curve at the symmetry point between the positive and negative bias currents. Its temperature dependence is predicted by the theory of variable range hopping,[4] with a Coulombic gap for the density of states, as

$$R(T) = R_0 \exp \sqrt{\frac{\Delta}{T}} \qquad (1)$$

where R_0 and Δ are constants and T is temperature.

As shown in Fig. 4, the experimental temperature dependence of the zero bias resistances are well described by Eq. (1). The straight line fit to the data matches very well over five orders of magnitude in resistance, in agreement with Eq. (1). However, despite the fact that both thermistors were made on the same chip and have very similar geometries, the fitted values for Δ are different, as are the R_0 values (Δ_a=7.667K, Δ_b=6.760K, R_{0a}= 0.060Ω, R_{0b}=0.0435 Ω). Similar phenomena have been observed on another sample.[8] Because of the doping method, we do not believe that this difference in resistance (about 50%) is due to variation of the dopant concentration. Other causes, such as stress, unannealed radiation damage and dislocations may affect the resistivity at these very low temperatures. We will show later that the heat capacities of the two thermistors are also significantly different.

3.3 Thermal Conductance between Sample and Heat Sink

If the phonons in the sample have a temperature T_{ph}, and the sink has a temperature T_0, then the power transmitted through the interface, P, can be modeled by

$$P = g_{ph\text{-}s} (T_{ph}{}^{\beta+1} - T_0{}^{\beta+1}) \qquad (2)$$

where T is temperature and β and $g_{ph\text{-}s}$ are constants. This leads to a thermal conductance, $G_{ph\text{-}s}(T)$, between the sample and the heat sink given by

$$G_{ph\text{-}s}(T) = \frac{dP}{dT_{ph}} = g_{ph\text{-}s}\,(\beta+1)\,T^{\beta} \qquad (3)$$

By measuring the power flow P and the temperatures T_{ph} and T_0, we can extract the values for $g_{ph\text{-}s}$ and β.

These measurements are made by applying a voltage V_{heat}, or heating power $P= I_{heat} V_{heat}$, to one thermistor (heating thermistor), and measuring the I-V curve of the other (monitoring thermistor). The zero bias resistance of the monitoring thermistor gives the phonon temperature T_{ph}:

$$T_{ph} = \frac{\Delta}{[\ln(\frac{R(I=0)}{R_0})]^2} \qquad (4)$$

where Δ and R_0 are values for thermistors a or b, depending on which thermistor is the monitor. To check if there is any noticeable temperature gradient between the phonons in the whole chip, the roles of heating and monitoring thermistors are exchanged .

In Fig. 5, we plot the heating power P_{heat} as a function of $(T_{ph}^{\beta+1} - T_0^{\beta+1})$ with the best fit $\beta = 3.2 \pm 0.1$ and $g_{ph\text{-}s} = 6.8\text{x}10^{-5}$ W/K$^{4.2}$. Notice that the data are taken at two different mixing chamber temperatures resulting in an equally good fit. All the data lie on a straight line, indicating that $g_{ph\text{-}s}$, the slope of this line, is independent of temperature. Furthermore, $g_{ph\text{-}s}$ is the same regardless of which thermistor is heated, indicating that there is no noticeable temperature gradient among the phonons within the entire chip.

3.4 I-V Nonlinearities

As shown in Fig. 3, the I-V curves at low temperatures are very nonlinear. This effect has also been seen by other groups at higher temperatures, though less pronounced.[9] Two basic explanations have been proposed: the resistance may have a strong electric field dependence, or electrons may decouple from phonons at these low temperatures, resulting in the "hot electron" effect (to simplify the notation, we use the term electron when describing a charge carrier).

3.4.1 Electric Field Model

The electric field effect model[9,10] assumes that the electrons and phonons have the same temperature, and that the resistance at non-zero bias depends not only on the temperature, but also on the electric field across the sample. The resistance at any bias is given by

$$R(E,T) = R_0 \exp\sqrt{\frac{\Delta}{T}} \exp\left(-\frac{eEL}{k_B T}\right) \qquad (5)$$

where E is the electric field across the sample, e is the electron charge, T is the temperature, k_B is Boltzmann's constant and L is a characteristic "hopping length".

Since the thermal conductance between the sample and the sink has already been measured, the phonon temperature T_{ph} can be obtained from the dissipated power in the thermistor, P=IV, from Eq. (2). The electrical field E is just $\frac{V}{t}$, where V is the voltage across the thermistor and t is the thermistor's thickness . The hopping length L can thus be deduced from Eq. (5). Because T_{ph} is not a constant along an entire I-V curve, one can obtain L as a function of temperature from a single I-V curve.

We show in Fig. 6 a plot of "hopping length" L vs. T_{ph} for thermistor a at four different mixing chamber temperatures. The temperature dependence of L does not follow

the $T^{-1/2}$ dependence predicted by the theory of variable range hopping. Moreover, the plot shows us that L appears to depend on the mixing chamber temperature, which is unphysical. Hence we conclude that our data cannot be explained in a simple fashion by the dependence of the resistance on the electric field.

3.4.2. Electron-Phonon Decoupling: A Thermal Model

At low temperatures, it is expected that the electrons and the phonons will thermally decouple since the phonon emission and absorption rate by electrons is proportional to the number of available final states for the electrons and phonons. At low temperatures, the number of available final states diminishes, resulting in a "hot electron" effect, which has been observed and is well understood in metals.[11-18] If power is applied to the electrons, we then expect the electrons in our sample to have a higher temperature than the phonons. We parameterize this effect by assuming that a finite thermal conductance $G_{e\text{-}ph}$ exists between the electrons and the phonons (Fig. 7), and that the resistance at any bias current depends only on the electron temperature, i.e.,

$$R(I,T) = R(T_e) = R_0 \exp\sqrt{\frac{\Delta}{T_e}} \qquad (6)$$

where T_e is the electron temperature.

In the steady state, which corresponds to any point on an I-V curve , the power dissipated in the thermistor, P = IV, has to flow from the electrons to the phonons, which we parameterize by

$$P = IV = g_{e\text{-}ph} (T_e^{\alpha+1} - T_{ph}^{\alpha+1}) \qquad (7a)$$

where $g_{e\text{-}ph}$ and α are constants. The same power has to flow from the phonons to the heat sink, which is expressed by Eq. (2), reproduced here:

$$P = g_{ph\text{-}s} (T_{ph}^{\beta+1} - T_0^{\beta+1}) \qquad (7b)$$

For this model to work, Eq. (7a) must be satisfied for certain values of α and $g_{e\text{-}ph}$ together with the already measured values of β and $g_{ph\text{-}s}$.

Figure 8 is a plot of P as a function of $(T_e^{\alpha+1} - T_{ph}^{\alpha+1})$ at four different mixing chamber temperatures for thermistor a. The data from different mixing chamber temperatures lie on the same straight line except those at very low power, indicating that $g_{e\text{-}ph}$ is independent of temperature. Similar data were also obtained for thermistor b. However, despite the fact that thermistors a and b are made on the same chip and have similar geometry, the best fit value of α for thermistor a is $\alpha = 5$, while that for thermistor b is $\alpha = 4.5$, and $g_{e\text{-}ph} = 0.0080\ W/K^6$ for thermistor a and $g_{e\text{-}ph} = 0.0013 W/K^{5.5}$ for thermistor b. This difference could be related to the fact that thermistors a and b have different Δ and R_0 values.

4. AC Measurements and Results

If our interpretation of the nonlinearity is correct, then the thermal decoupling model should describe not only the static behavior, but also the dynamic behavior of the sample when we apply an electrical pulse to the sample. In this section, we compare the observed response of thermistor a to electrical pulses with the predictions of the thermal model proposed above, which in turn allows us to determine the heat capacity of the electrons.

4.1 Experimental Setup and Method

The circuit for AC measurements is shown in Fig. 9. Large stray capacitances C_s (660-900pF) are due to the wiring of the refrigerator. As in the DC case, all the amplifiers

and the bias circuit are placed inside the screen room and powered by batteries, and rf filters (with about a 1MHz cutoff frequency) are used on all the leads to the sample. An RC filter is used at the output of the function generator to eliminate high frequency noise.

One of the purposes of the AC measurement is to determine the heat capacity of the electrons. The electron heat capacity in a thermistor is found by depositing a small amount of energy in the thermistor and measuring the resulting temperature change. The energy is deposited by applying a square-wave pulse of amplitude ΔV and width 100 ms through a series capacitor C_1 of 20 pF to the thermistor biased at a constant current. The temperature change of the thermistor is determined from the change of resistance caused by the heating. The width of the input square-wave signal (100ms) is chosen to be much longer than any of the thermal or electrical time constants in the system. The response of the thermistor is measured for various DC bias currents and a range of pulse heights, ΔV. These measurements were made at several mixing chamber temperatures. All the voltage responses were recorded on a digital oscilloscope.

4.2 Prediction of the Thermal Model

When the thermistor in Fig. 9 is biased at a constant current and is given a square wave signal of amplitude ΔV through C_1, its response consists of both an electrical effect and a thermal effect. If the thermistor's resistance R were constant with temperature, then only the electrical effect would be observed: a pulse of initial height $V_0 + \frac{C_1}{C_s + C_1}\Delta V$, where V_0 is the bias voltage across the thermistor, followed by an exponential decay to V_0 with a time constant $\tau_e = R(C_s+C_1)$.

The thermal effect is due to the fact that the resistance is temperature dependent. Assume that the electrical time constant τ_e is much less than the thermal time constant $\tau_{th} = \frac{c}{G_{e\text{-}ph}}$, where c is the heat capacity of the electrons. When energy is deposited in the

thermistor at the start of the pulse, the temperature of the thermistor increases and the resistance drops; this in turn causes the voltage measured across the thermistor to drop. For small energy deposition, the drop ΔV_{th} is proportional to $\frac{\Delta E}{C}$, where ΔE is the energy deposited. The heated thermistor then cools to the original temperature with a thermal time constant τ_{th}. The observed voltage thus consists of an initial drop followed by a decay to the bias voltage V_0.

In the real system, both the electrical and the thermal effects exist. The voltage response of the thermistor is a combination of the two effects described above.

The heat capacity is obtained by fitting the thermal model to the observed data. The temperature dependence of the heat capacity has to be known to calculate the full response. However, if the temperature change is so small that the heat capacity does not change significantly, then ΔV_{th} depends on ΔE linearly in good approximation, and only the value of the heat capacity at the electron temperature is required for the calculation. Therefore the fit yields the heat capacity at some particular temperature. Details of the calculation are contained in the Appendix.

4.3 Data and Fit

Figures 10a and 10b show two examples of the observed voltage response and the fit. Both figures indicate that the thermal model matches the data very well, both in the pulse height and the pulse shape. Notice the model even matches the oscillating behavior displayed in Fig. 10a. The oscillating behavior is due to the thermal-electric feedback.

Similar fits were done at different bias currents, i.e., at different electron temperatures, and for both thermistors a and b. To make sure that the temperature change is small, we checked that ΔV_{th} depends on ΔE linearly. Figure 11 is the plot of heat capacity, extracted from the fits at different bias and mixing chamber temperatures, vs.

electron temperature for both thermistors a and b. The plot clearly indicates that the temperature dependence of thermistor a's heat capacity is stronger than linear, while that of thermistor b is about linear. Unfortunately, the temperature span is not wide enough for us to determine the temperature dependences.

5. Discussion

5.1 Prediction of I-V Curves

Because both $g_{e\text{-}ph}$ and $g_{ph\text{-}s}$ are independent of temperature, in principle they can be obtained from I-V measurements and measurements of the Kapitza thermal conductance made at one mixing chamber temperature T_0. I-V curves at any other mixing chamber temperatures can then be calculated based on the thermal model.

The calculation of an I-V curve is performed in the following way. At some mixing chamber temperature T_0 and for a given current I, the equilibrium values of T_e and T_{ph} can be found by solving the following equations, provided $R(T_e)$ is known:

$$I^2 R_0 \exp\sqrt{\frac{\Delta}{T_e}} = g_{e\text{-}ph}\,(T_e^{\alpha+1} - T_{ph}^{\alpha+1}) = g_{ph\text{-}s}\,(T_{ph}^{\beta+1} - T_0^{\beta+1}) \qquad (8)$$

The corresponding voltage is given by:

$$V = I\,R_0 \exp\sqrt{\frac{\Delta}{T_e}} \qquad (9)$$

Thus a full I-V curve can be generated at any desired mixing chamber temperature. In Fig. 12, we show the I-V curves calculated from the thermal model and the measured ones of thermistor a. One can see that the predicted I-V curves have the basic features of the measured ones; for instance, the maximum on the I-V at low T_0, the overall structure and

the absolute scale. However, deviations are observed at small currents and at low temperatures, which could be due to our approximate parameterization.

5.2 Results of the AC Measurements

The difference in heat capacity between thermistors a and b is very surprising because they are both on the same chip. Whether or not this difference is related to their difference in resistance is not yet clear.

On the other hand, the temperature dependence of thermistor a's heat capacity is not too surprising. In the theory of variable range hopping, electrical conduction only requires that percolation paths be connected from one side of the sample to the other in the direction of the electrical field, which could involve only a small number of electrons, not all of them. Therefore it is possible that only the electrons that participate in the electrical conduction contribute to the heat capacity. More studies are needed to arrive at a thorough understanding of this phenomenon.

6.Conclusions

We have measured the electrical resistance, thermal conductance, and heat capacity of NTD Ge #12 near 20 mK. The theory of variable range hopping explains the temperature dependence of the zero bias resistance very well . The I-V curves and the dynamic behavior of the thermistors are well described by the thermal decoupling between the electrons and the phonons.

If our interpretation is correct, our data imply that the decoupling between the electrons and the thermal phonons limits the expected gain of a thermistor operating at low temperatures. Moreover, we would expect that high energy phonons (ballistic phonons) couple better to the electrons because the available final states of the high energy phonons

occupy a larger volume in phase space. Good coupling between high energy phonons and electrons is required to detect high energy phonons with a thermistor.

Acknowledgement

We are very grateful to J. Clarke, A. Cleland, A.Cumming, T. Kenny, A. Lange, P.Luke, P. Richards, R.Ross, T. Shutt, and H. Steiner for their generous help and/or valuable comments. This work is supported by US Department of Energy under contract DE-AC03-76SF00098.

Appendix

The voltage response of a thermistor to an electrical pulse can be calculated from the electrical and thermal circuits of the thermistor.

The electrical circuit of a thermistor in Fig. 9 can be simplified to Fig. 13, where R_{bias}, R_{th}, and R_w are the resistances of the bias resistor, the thermistor and the wire, respectively; C_1 and C_s are the coupling and stray capacitances, respectively; V_{bias} is the bias voltage, and ΔV is the signal from a pulse generator. From simple circuit theory, we obtain

$$RC\frac{dV_{th}}{dt} + V_{th} = \frac{R_s}{R_t} V_{bias} + \frac{R_s R_{bias}}{R_t} C_1 \frac{d(\Delta V)}{dt} \qquad (1)$$

where $RC = \frac{R_s R_{bias}}{R_t} (C_1 + C_s)$, $R_t = R_s + R_{bias}$, and $R_s = R_{th} + R_w$. Note that R_{th}, and therefore R_s and R_t, are functions of temperature.

The basic thermal circuit of a thermistor is shown in Fig. 7. However, at low temperatures, the thermal conductance between the electrons in the contacts (the Au, the B^+ implant, and the epoxy), and the phonons in the sample is finite. A more accurate thermal circuit is shown in Fig. 14, where $G_{e\text{-}ph}$, $G_{ph\text{-}s}$, and $G_{g\text{-}ph}$ are the thermal conductances between the electrons and the phonons, the phonons and the thermal sink, the phonons and the contacts, respectively. We take the functional forms of the various conductances to be $G_{e\text{-}ph} = g_{e\text{-}ph}(T_e^{\alpha} - T_{ph}^{\alpha})$, $G_{ph\text{-}s} = g_{ph\text{-}s}(T_{ph}^{\beta} - T_0^{\beta})$, and $G_{g\text{-}ph} = g_{g\text{-}ph}(T_g^{\gamma} - T_{ph}^{\gamma})$. We also assume that the Au, the B^+ implant and the epoxy have the same temperature, and that

their only thermal connection to the electrons or to the sink is through the phonons. This is a good approximation for small ΔV, but not as good for large ΔV.

From conservation of energy, we obtain the following equations:

$$\frac{dq}{dt} - g_{e\text{-}ph} \left(T_e^{\alpha} - T_{ph}^{\alpha} \right) = C_e (T_e) \frac{dT_e}{dt} \qquad (2)$$

$$g_{g\text{-}ph} \left(T_{ph}^{\gamma} - T_g^{\gamma} \right) = C_g (T_g) \frac{dT_g}{dt} \qquad (3)$$

$$g_{e\text{-}ph} \left(T_e^{\alpha} - T_{ph}^{\alpha} \right) - g_{g\text{-}ph} \left(T_{ph}^{\gamma} - T_g^{\gamma} \right) - g_{ph\text{-}s} \left(T_{ph}^{\beta} - T_0^{\beta} \right)$$

$$= C_{ph} (T_{ph}) \frac{dT_{ph}}{dt} \qquad (4)$$

where T_e, T_g, T_{ph}, and T_0 are the temperatures of the electrons, the epoxy-Au-B^+ implant, the phonons, and the mixing chamber, repectively; C_e,C_g, and C_{ph} are the heat capacities of the electrons, the epoxy-Au-B^+ implant, and the phonons, respectively; and q is the energy deposited in the electrons. For small pulses the results are not sensitive to the parameters for the epoxy-Au-B^+ implant subsystem. We thus assume that the thermal conductivity between the phonons in the sample and the subsystem is the same as that between the phonons and the thermal sink. The only difference in the thermal conductance is then in the contact area, so we have $g_{g\text{-}ph} = 3 \cdot g_{ph\text{-}s}$ and $\gamma = \beta$. The parameters $g_{e\text{-}ph}$, $g_{ph\text{-}s}$, α, and β are determined from experimental measurements.

For a step function excitation $\Delta V(t) = \Delta V \cdot \theta(t)$, where

$$\theta(t) = 1 \quad t > 0$$

$$= 0 \quad t \leq 0$$

$V_{th}(t)$ can be calculated from the above four equations by integrating in time; fine steps have to be used for convergence. For small energy depositions, the response is linear in the excitation (ΔV) , and by fitting the maximum calculated pulse height $V_{th}(t)$ to the observed data, we obtain the electron heat capacity. If our description of the dynamic behaviour of the system is correct, in particular if the thermal conductances are real, we should obtain the observed pulse shape and time constant, as we do.

Figure Captions

1) The double thermistor sample used in the experiment. It is made of NTD Ge #12, and thermistor a is glued to the heat sink with conductive epoxy.

2) The circuit used for the I-V measurements, where V_{bias} is the bias voltage that supplies the current to the thermistor, R_{bias} = 10 MΩ, R_{th} is the resistance of a thermistor, I_{th} and V_{th} are the current and voltage of the thermistor.

3) I-V curves of NTD Ge #12 (sample #01,thermistor a) at four different mixing chamber temperatures denoted by T_0. Note the nonlinearity of the I-V curves.

4) Temperature dependence of the resistance of NTD Ge #12 at zero bias current (sample #01,thermistor a and b), where T is the mixing chamber temperature and the solid lines are the best fits to the data.

5) Measurements of Kapitza thermal conductance at two mixing chamber temperatures. T_{ph} is the phonon temperature of the sample, T_0 is the mixing chamber temperature. The solid line is the best fit to the data.

6) Hopping length deduced from the electrical field effect model as a function of the thermistor's temperature, i.e., the phonon temperature, at four different mixing chamber temperatures denoted by T_0.

7) A box diagram of the thermal model. Electrical power P=IV is applied to an electron system, which is coupled to a phonon system through a thermal conductance $G_{e\text{-}ph}$. The phonons are connected to a heat sink by a thermal conductance $G_{ph\text{-}s}$.

8) Measurements of the thermal conductance between the electrons and the phonons in thermistor a (NTD Ge #12,#01) at four mixing chamber temperatures. The solid line is the best straight line fit to the data.

9) The electrical circuit used for the AC measurements. A square voltage pulse of amplitude ΔV and width of 100 ms is applied to a thermistor through a capacitor C_1= 20 pF. The voltage across the thermistor is amplified, filtered and recorded. C_s is a stray capacitance of the order 600-900 pF.

10) Comparison of the voltage response of thermistor a with the prediction of the thermal model at two electron temperatures. The solid lines are the predictions and the points are the data. The difference in the rise time at t=0 is mainly due to the limited bandwidth of the amplifier. a):T_0 =18.8 mK, I=2.nA, T_e = 28.3mK, ΔE=67eV, heat capacity = 3.2×10^{-13} J/K; b):T_0 = 33.2 mK, I=20.nA, T_e = 41.2 mK, ΔE=3.4keV, heat capacity = 2.8×10^{-12} J/K.

11) The estimate of the electron heat capacity of thermistors a and b as a function of electron temperature. The solid lines are not fits, but serve as guides. The points are the estimates obtained by fitting the thermal model to the observed thermal pulses.

12) Comparison of the observed I-V curves with the calculation based on the thermal model at four different mixing chamber temperatures. The solid lines are the results of our calculations.

13) The electrical circuit used in the calculation of a thermal pulse using the thermal model. C_1= 20 pF, R_{bias} = 10 MΩ, R_w = R_{wire} = 200 Ω, C_s = 660 pF for thermistor a and 900 pF for thermistor b.

14) The thermal circuit used in the calculation of a thermal pulse. $G_{e\text{-}ph}$ is obtained from the best fit in Fig. 8 for thermistor a (from a similar fit for thermistor b). $G_{ph\text{-}s}$ is obtained

from the best fit in Fig. 5. For small ΔV case, $G_{g\text{-}ph}$ is not very critical for the calculation because the phonon temperature hardly changes. We assume that the thermal conductivity between the contacts and the phonons is the same as that between the phonons and the thermal sink, then $G_{g\text{-}ph} = 3 \cdot G_{ph\text{-}s}$, where the factor 3 comes from the difference in contact area.

Reference

1 A.E.Lange, E.Kreysa, S.E.McBride, P.L.Richards, E.E.Haller, Int. J. IR + MM Waves 4, 689 (1983).

2 D.McCammon, M.Juda, J.Zhang, S.S.Holt, R.L.Kelley, S.H.Moseley, and A.E.Szymkowiak, Proc. 18th Int. Conf. on Low Temperature Physics, Kyoto,1987, Jap. Journal of Appl. Phys. 26, Supplement 26-30(1987).

3 A. Alessandrello, D.V.Camin, E.Fiorini, A.Giuliani, Phys.Lett. B 202, 611(1988).

4 A.L.Efros and B.I.Shklovskii, Electronic Properties of Doped Semiconductors (Springer-Verlag, New York, 1984), p.202.

5 B.Sadoulet, Proceedings of European Workshop on Low Temperature Devices for the Detection of Low Energy Neutrinos and Dark Matter (In press), LBL preprint 25725, (1988).

6 E.E.Haller, Infrared Phys. 25, 257(1985).

7 E.Kreysa, private communication.

8 N.Wang, B.Sadoulet, T.Shutt, J.Beeman, E.E.Haller, A.Lange, I.Park, R.Ross, C.Stanton, H.Steiner, IEEE Trans. on Nuclear Science,vol. 35, No.1, 55 (1988).

9 T.Kenny, P.L.Richards, E.E.Haller, and J.Beeman, Phys. Rev. B, to be published.

10 T.F.Rosenbaum, K.Andres, G.A.Thomas, Solid. State Commun. 35, 663(1980).

11 A.C. Anderson, J.H.Anderson, M.P.Zaitlin, Rev.Sci.Instrum. 47, 407(1976).

12 A.C.Anderson, Rev.Sci.Instrum. 51, 1603(1980).

[13] E.P.Roth, J.R.Matey, A.C.Anderson, and D.A.Johns, Rev.Sci.Instrum. 49, 813(1978).

[14] G.X.Mack, A.C. Anderson, P.R.Swinehart, Rev.Sci.Instrum. 54, 949(1983).

[15] W.A. Little, Can. J. Phys. 37, 334(1959).

[16] M.L.Roukes, M.R.Freeman, R.S.Gremain, R.C.Richardson and M.B.Ketchen, Phys. Rev. Lett. 55, 422(1985).

[17] A.C.Anderson and R.E.Peterson, Phys. Lett. 38A, 519(1972).

[18] F.C.Wellstood, C.Urbina, and J.Clarke, IEEE Trans. on Magnetics(1988) , to be pulished; presented at the Applied Superconductivity Conference in San Francisco, Aug.1988.

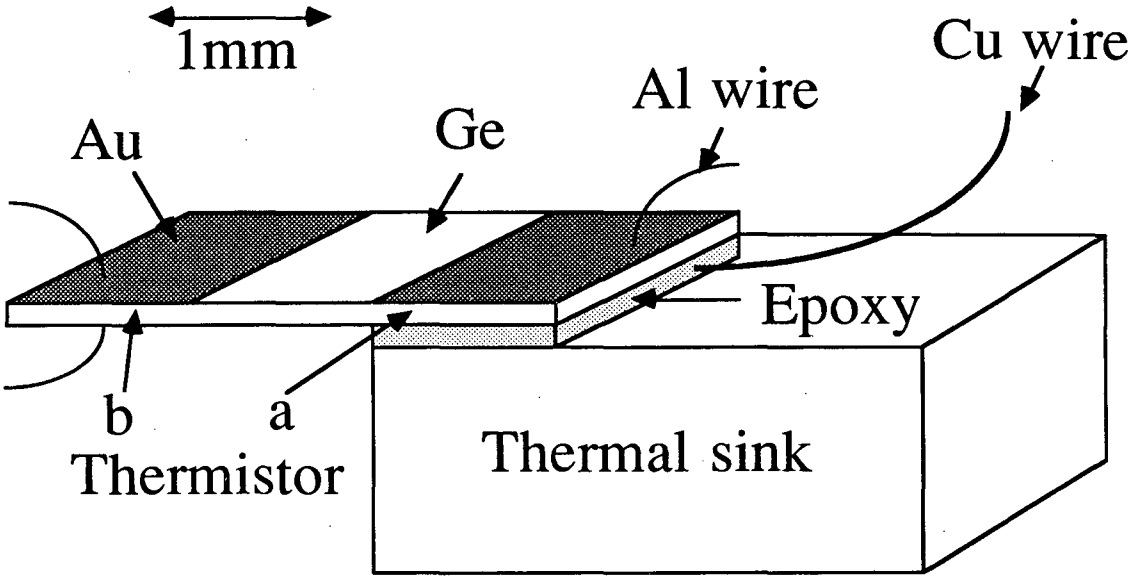
1mm
Cu wire
Al wire
Au
Ge
Epoxy
b
Thermistor
a
Thermal sink
XBL 892-520

Fig. 1

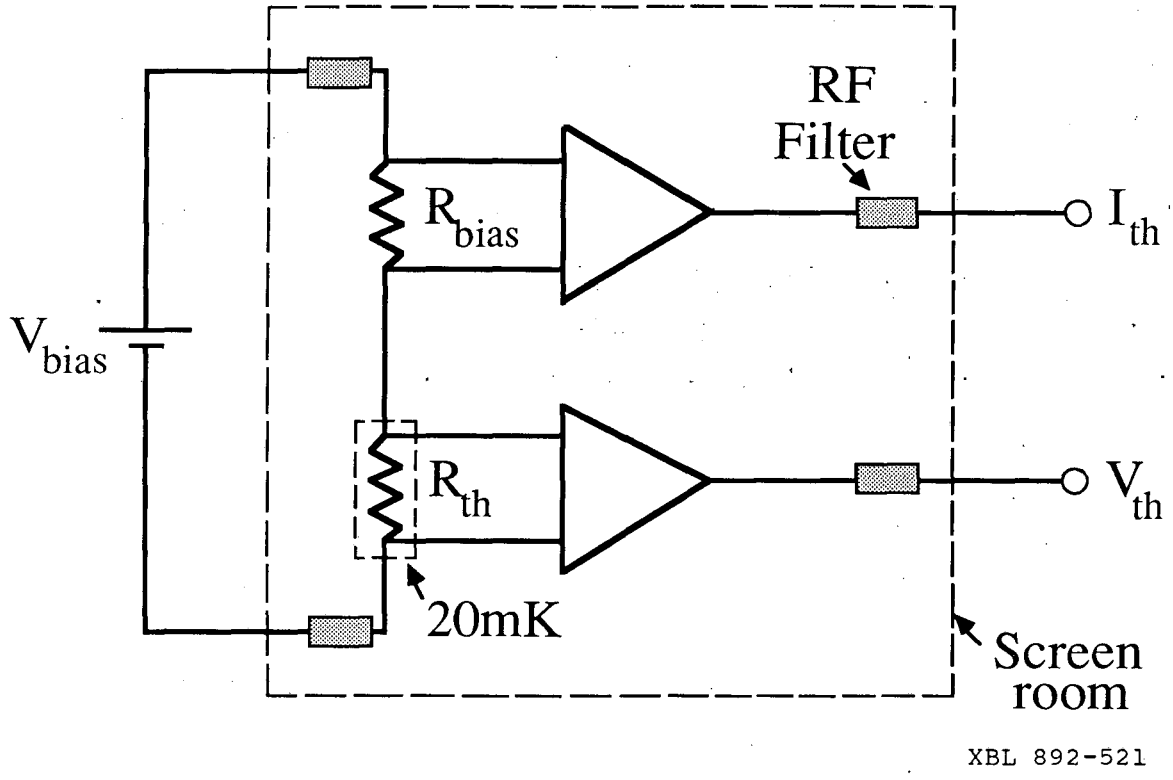
RF
Filter
R_{bias}
I_{th}
V_{bias}
R_{th}
V_{th}
20mK
Screen
room
XBL 892-521

Fig. 2

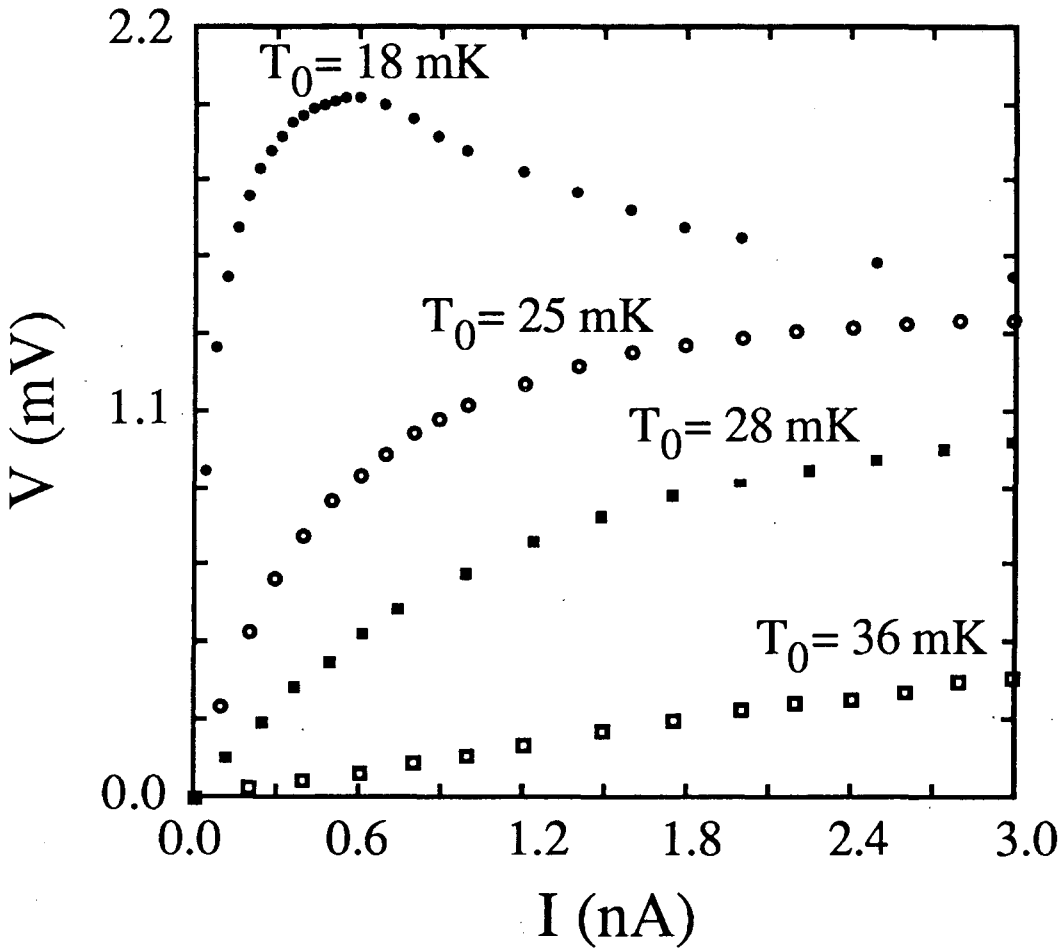

XBL 892-525

Fig. 3

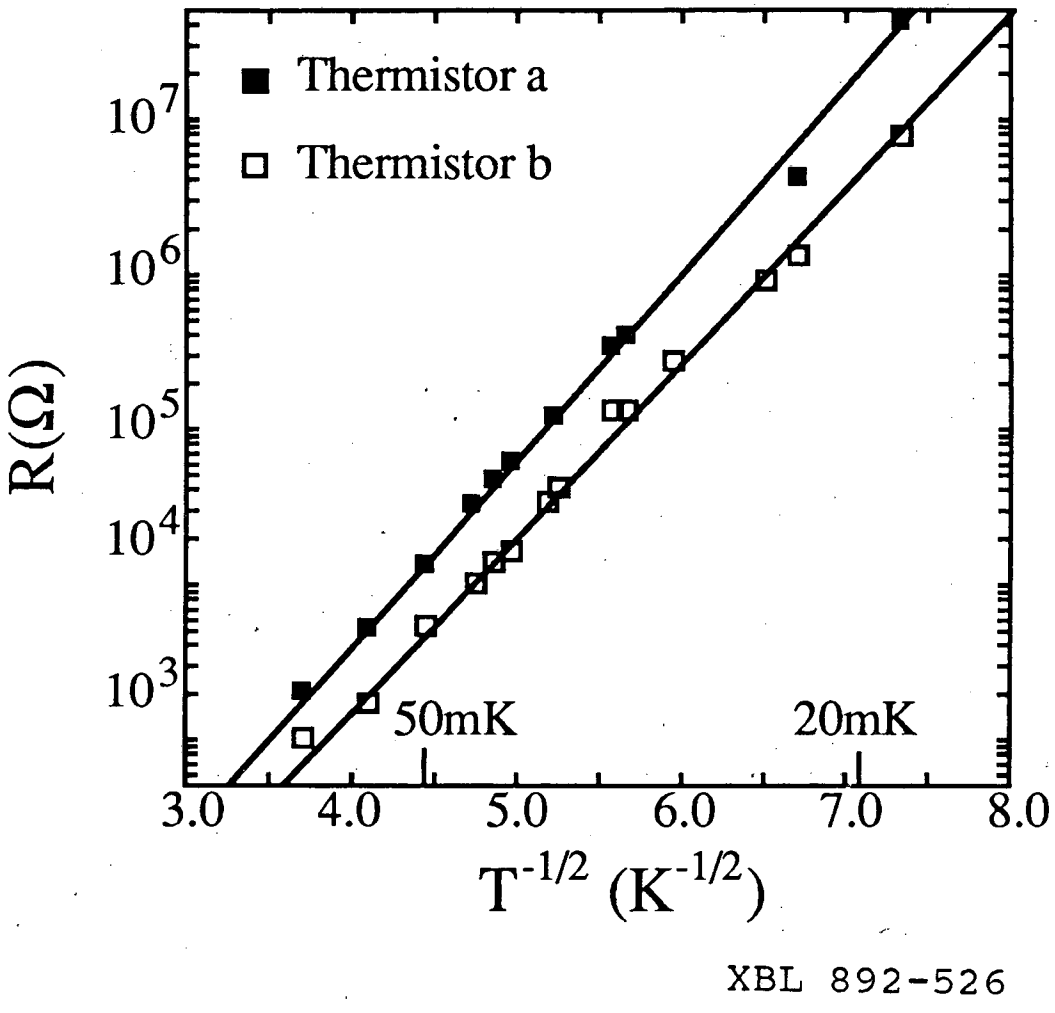
Thermistor a
Thermistor b
10^7
10^6
10^5
10^4
10^3
R(Ω)
50mK
20mK
3.0
4.0
5.0
6.0
7.0
8.0
$T^{-1/2}$ ($K^{-1/2}$)
XBL 892-526

Fig. 4

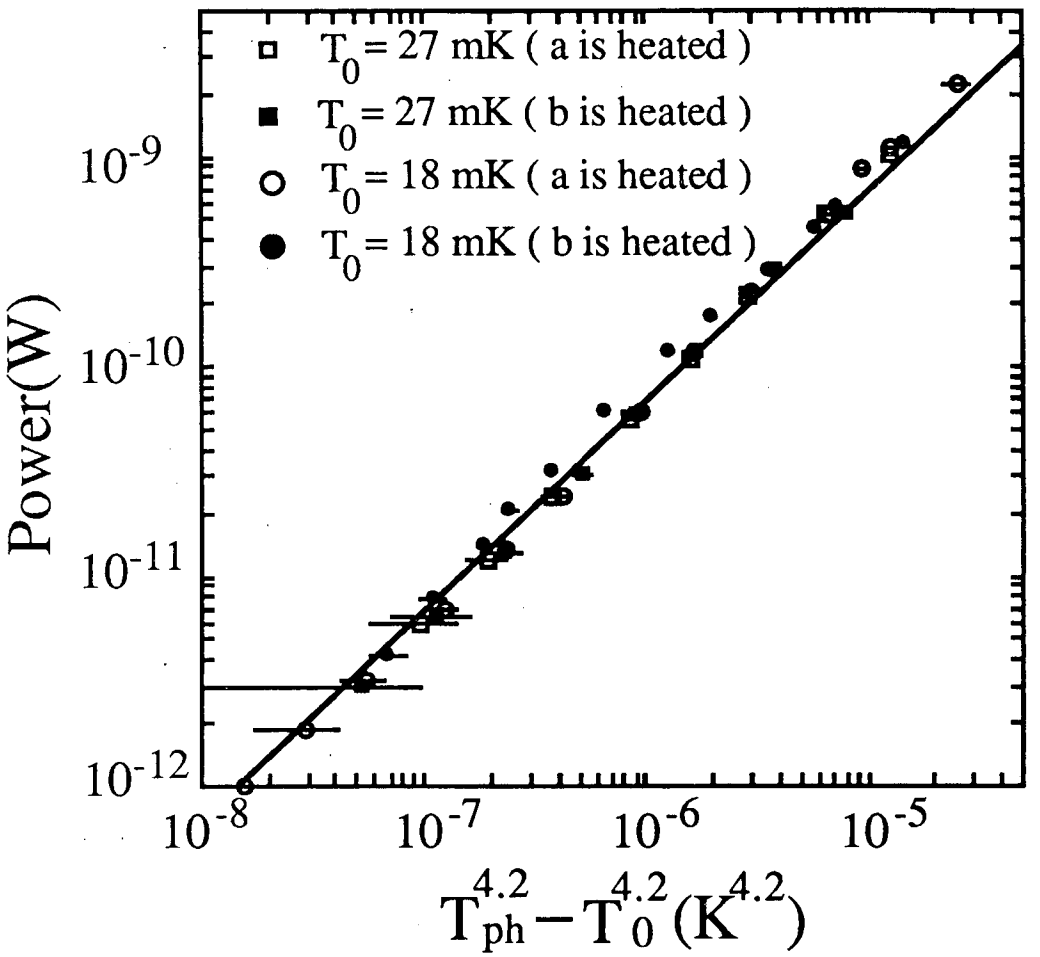

XBL 892-527

Fig. 5

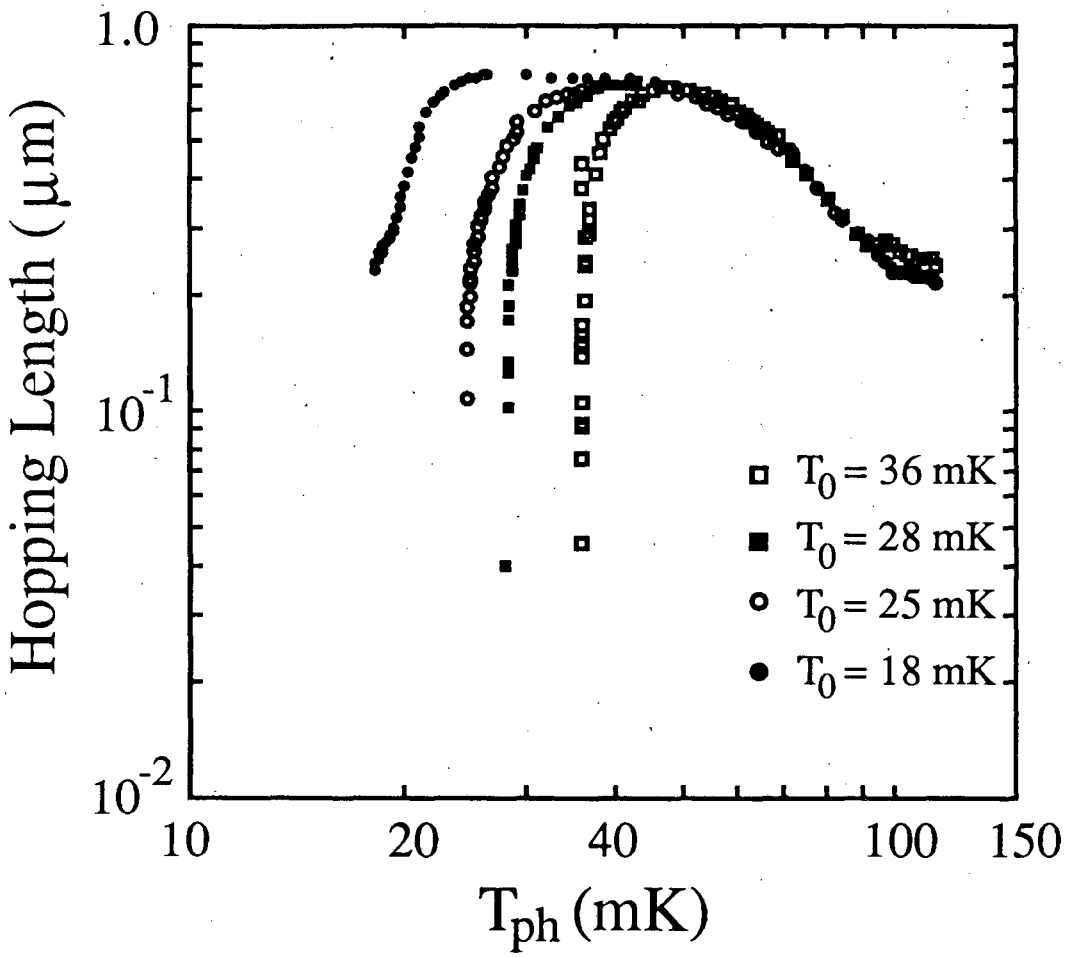

XBL 892-528

Fig. 6

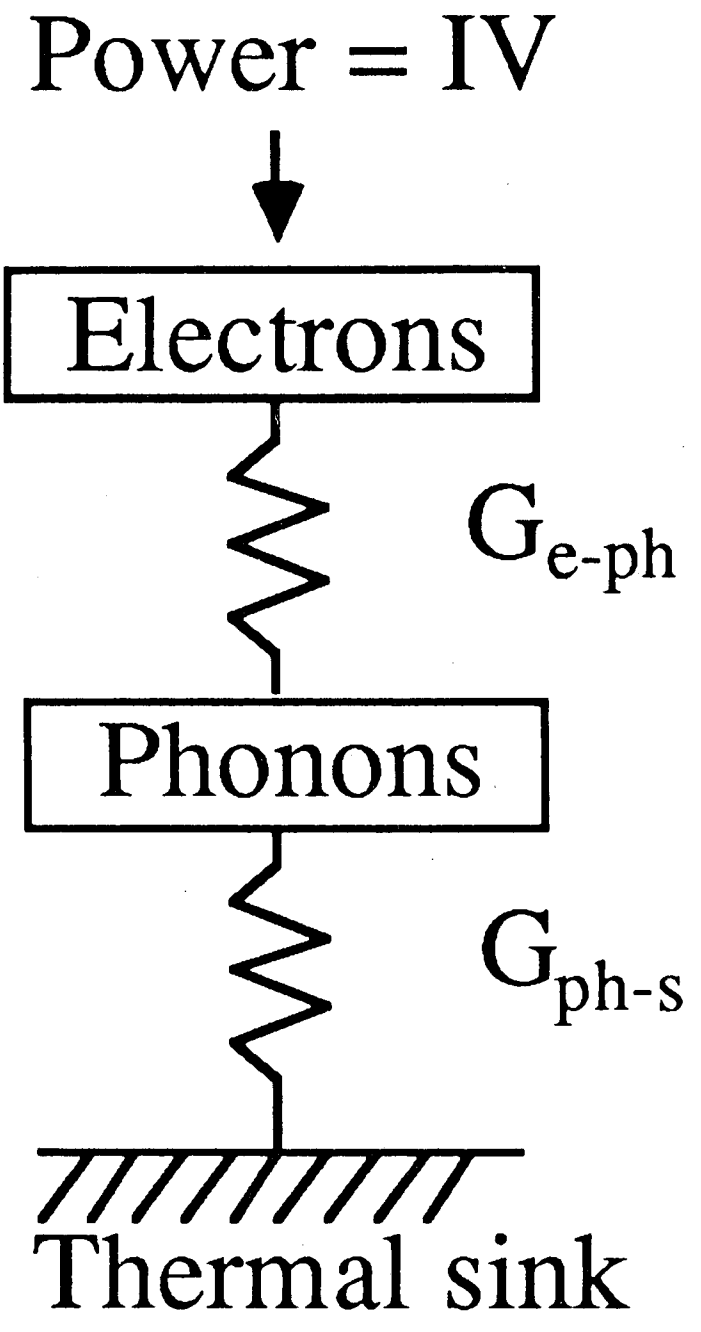

XBL 892-529

Fig. 7

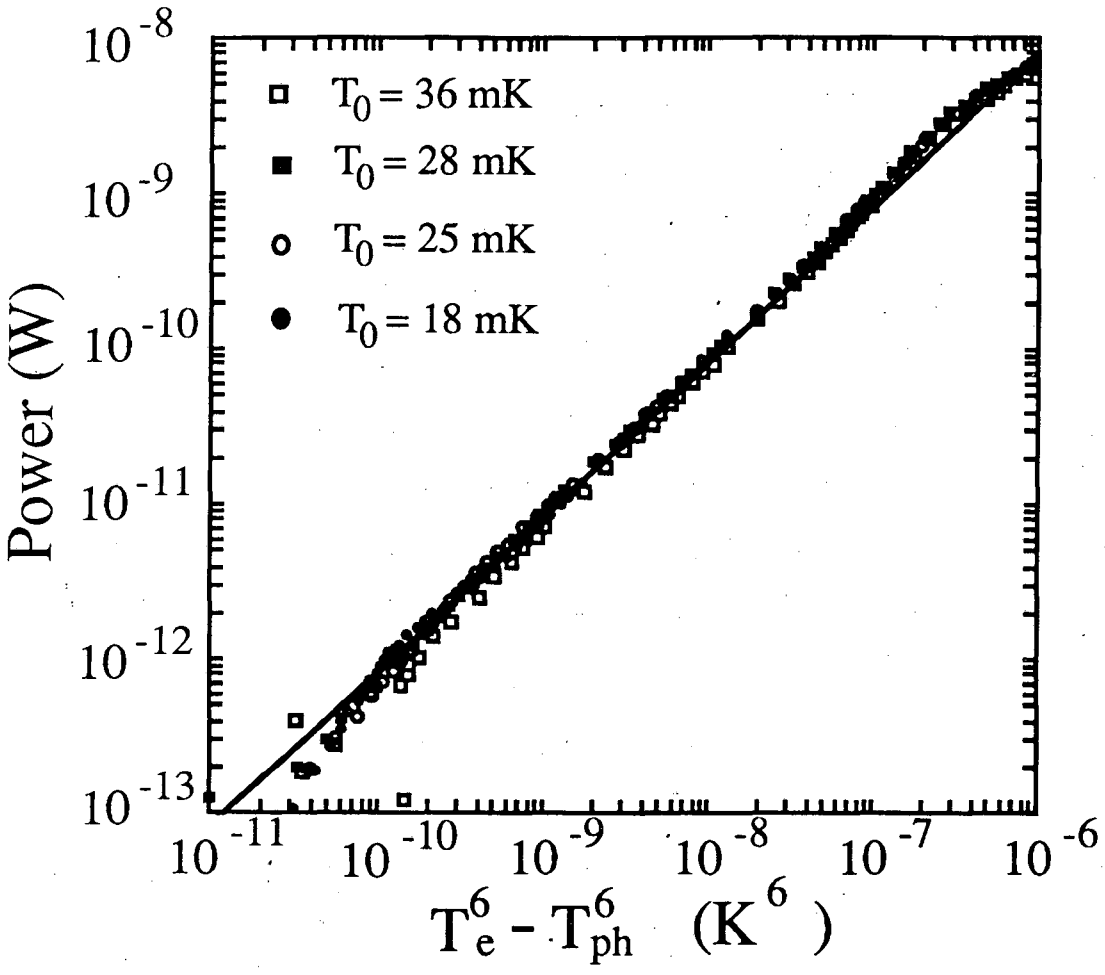
10^{-8}
10^{-9}
10^{-10}
10^{-11}
10^{-12}
10^{-13}
Power (W)
$T_0 = 36$ mK
$T_0 = 28$ mK
$T_0 = 25$ mK
$T_0 = 18$ mK
10^{-11}
10^{-10}
10^{-9}
10^{-8}
10^{-7}
10^{-6}
$T_e^6 - T_{ph}^6$ (K^6)
XBL 892-530

Fig. 8

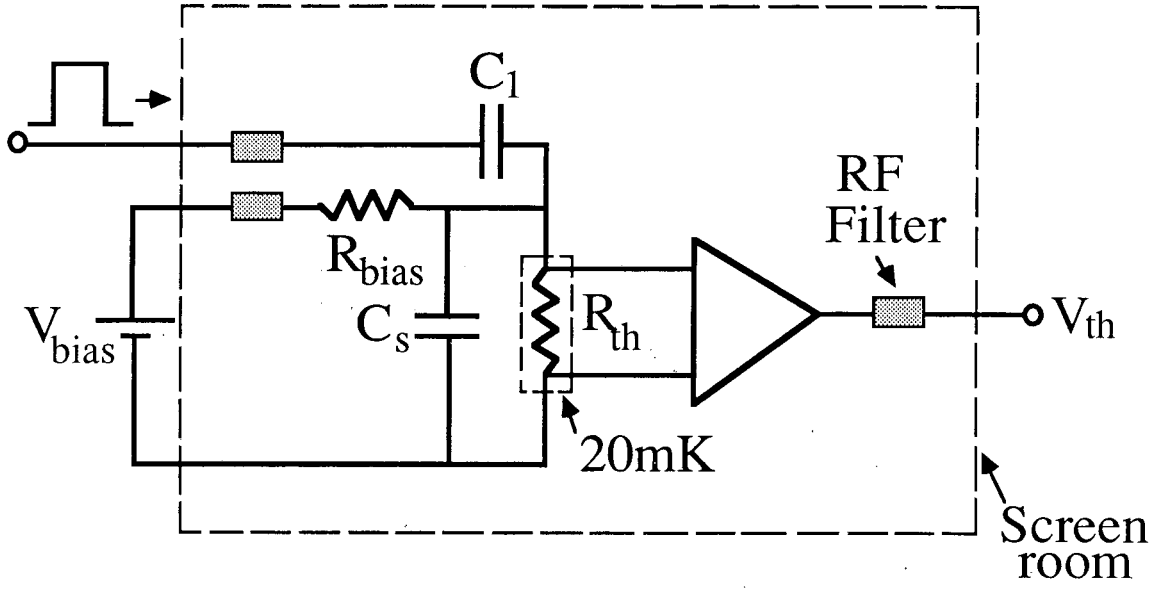

XBL 892-522

Fig. 9

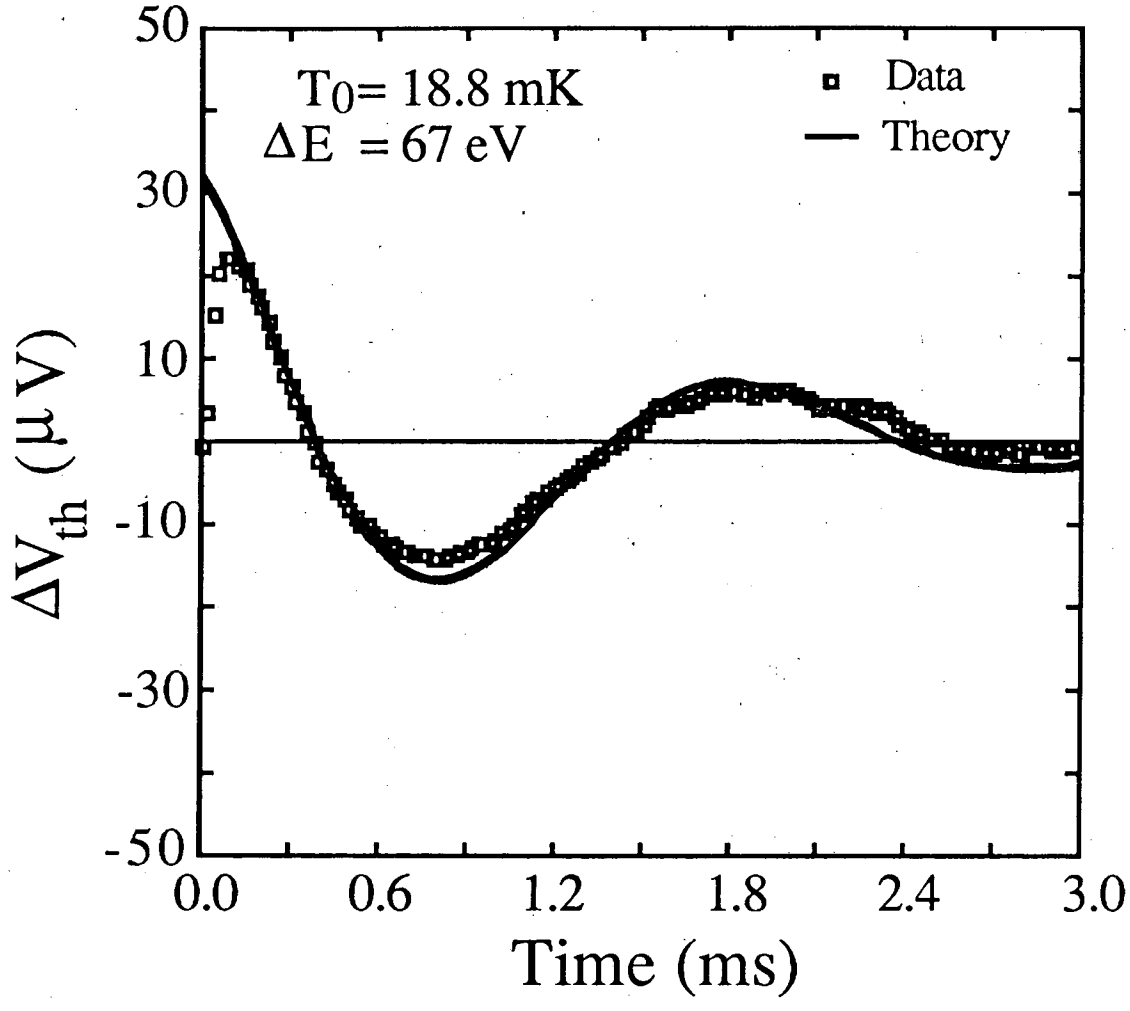

XBL 892-531

Fig. 10a

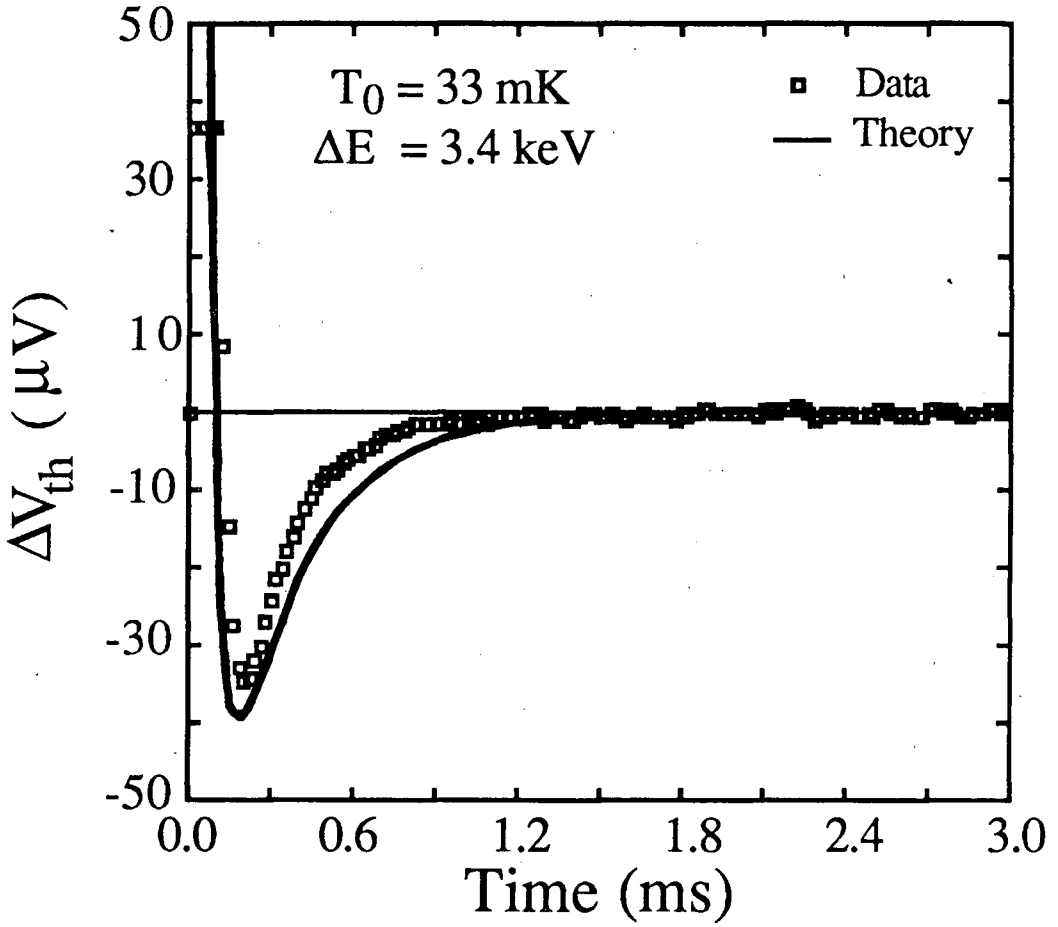
50
30
10
-10
-30
-50
0.0
0.6
1.2
1.8
2.4
3.0
Time (ms)
ΔV_{th} (μV)
T_0 = 33 mK
ΔE = 3.4 keV
Data
Theory
XBL 892-532

Fig. 10b

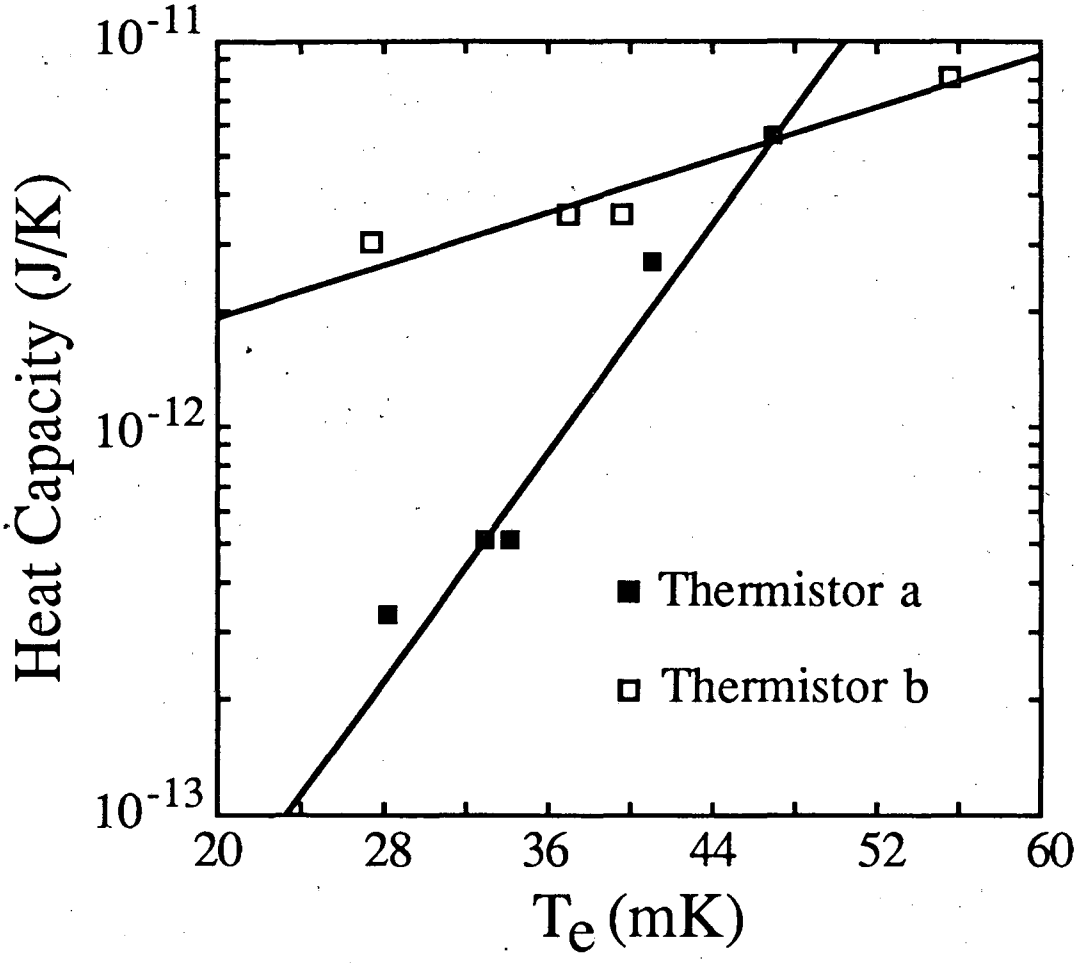

XBL 892-533

Fig. 11

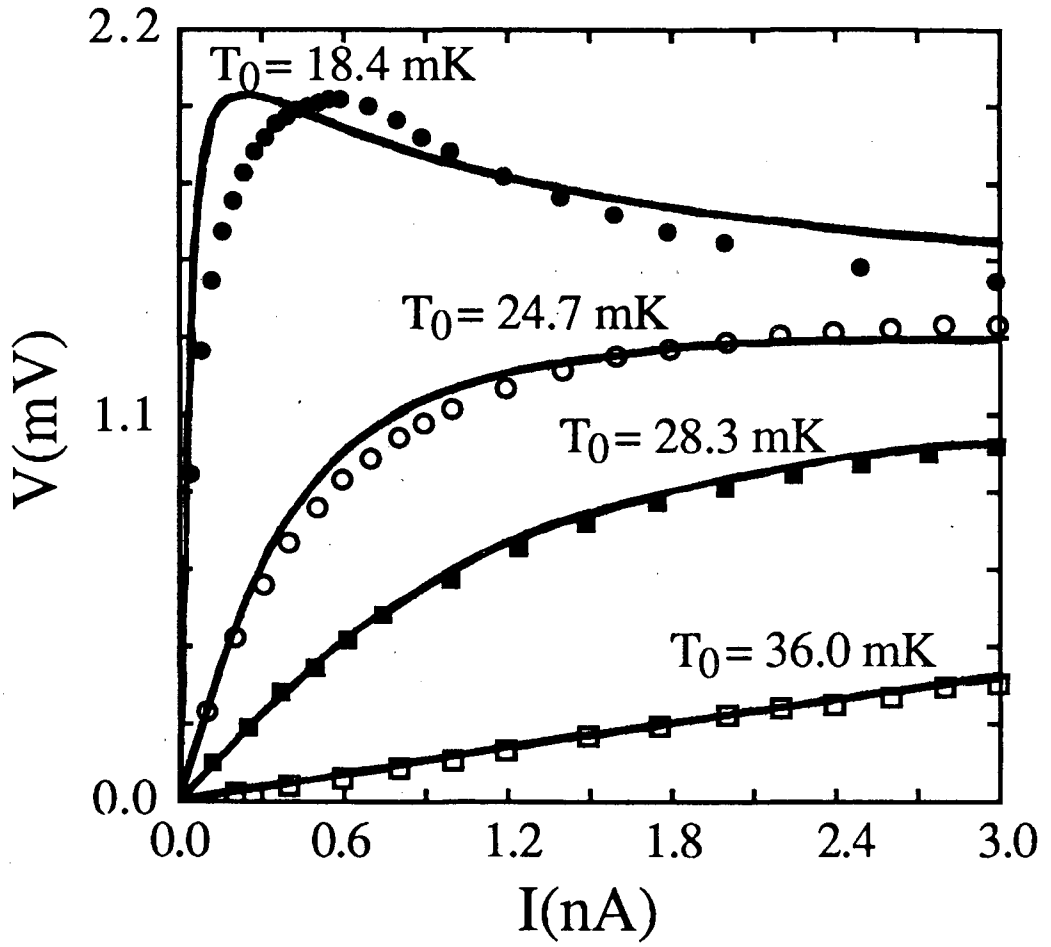

XBL 892-534

Fig. 12

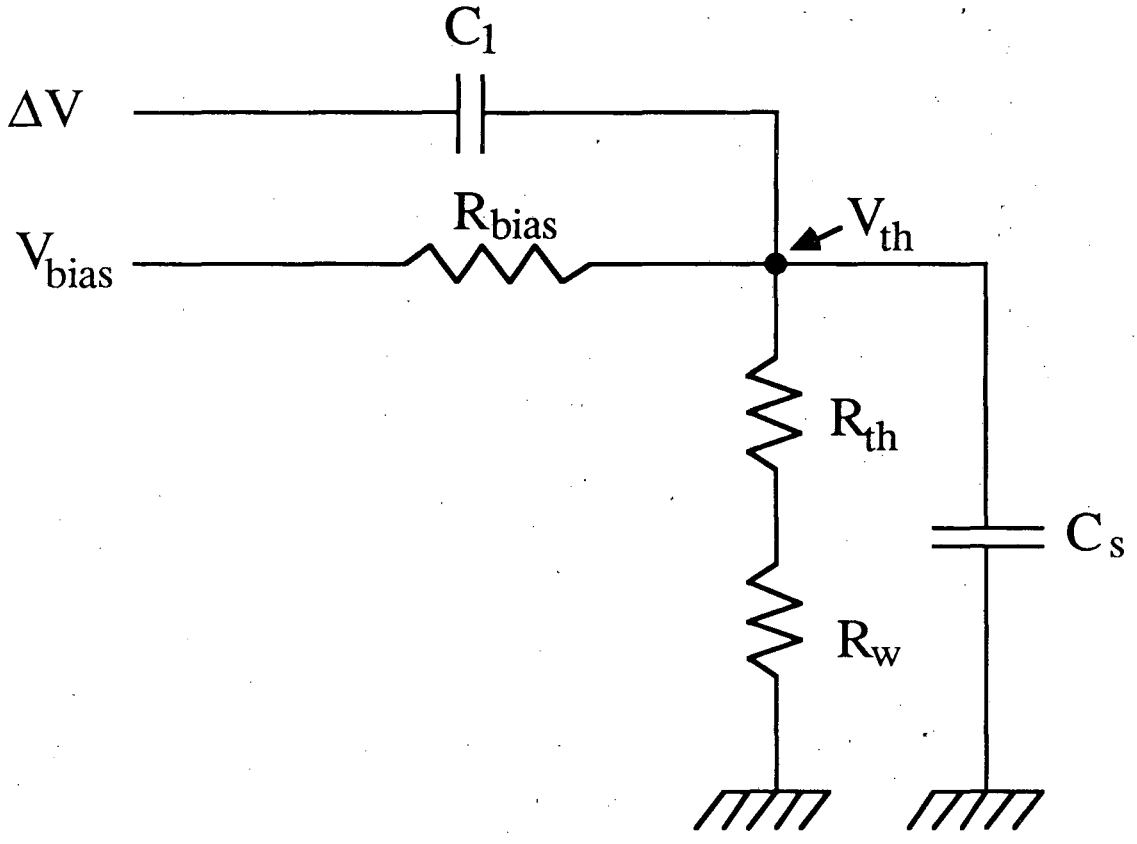

Fig. 13

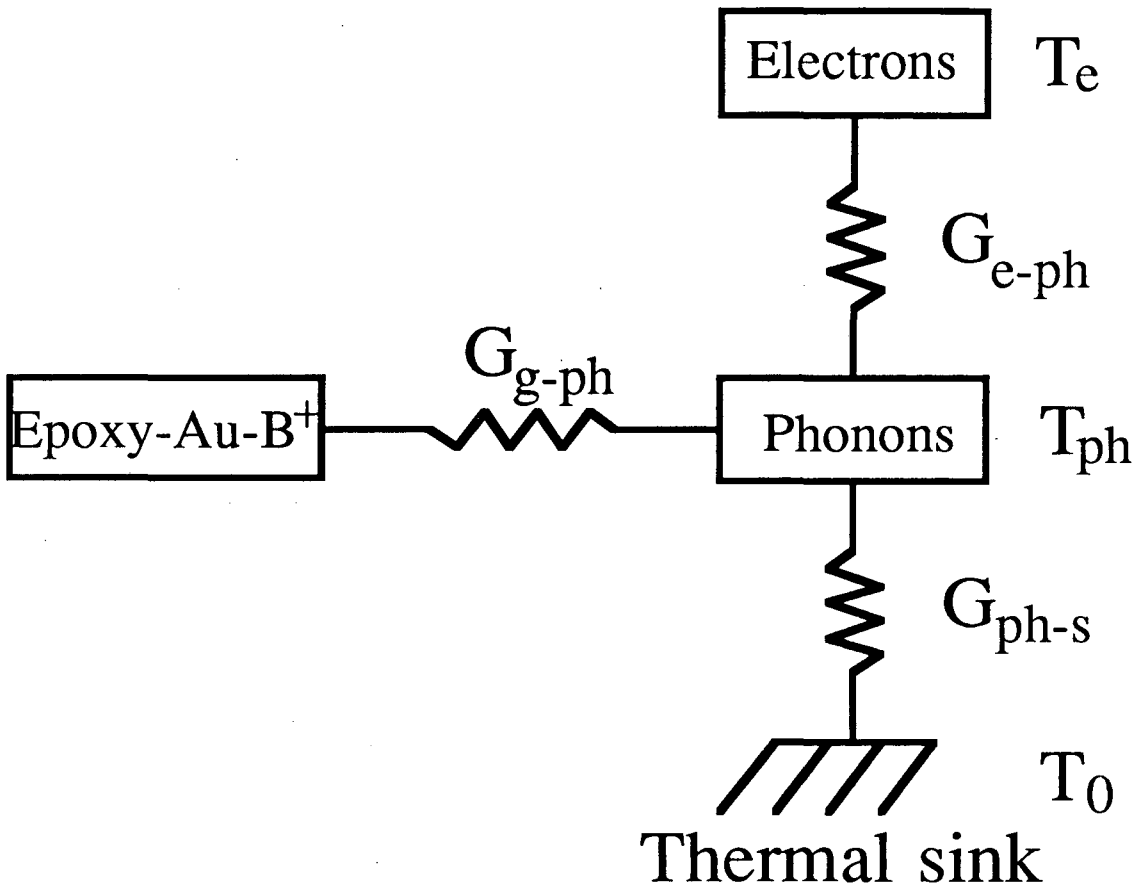
Electrons
T_e
$G_{e\text{-}ph}$
$G_{g\text{-}ph}$
Epoxy-Au-B^+
Phonons
T_{ph}
$G_{ph\text{-}s}$
T_0
Thermal sink
XBL 892-524

Fig. 14

LAWRENCE BERKELEY LABORATORY
TECHNICAL INFORMATION DEPARTMENT
1 CYCLOTRON ROAD
BERKELEY, CALIFORNIA 94720